Near-Real-Time Retrieval of Cloud Properties Over the ARM CART Area from GOES Data

P. Minnis, W. L. Smith, Jr., D. F. Young, and L. Nguyen
Atmospheric Sciences
National Aeronautics and Space Administration
Langley Research Center
Hampton, Virginia

A. D. Rapp, P. W. Heck, and M. M. Khaiyer
Analytical Services & Materials, Inc.
Hampton, Virginia

Introduction

Mesoscale cloud properties complement the point measurements of similar parameters at the Atmospheric Radiation Measurement (ARM) surface sites. To improve upon the climatology of satellite-derived cloud properties over the ARM Southern Great Plains (SGP) domain, a pair of multi-spectral algorithms, the Visible-Infrared-Solar Infrared-Split Window Technique (VISST) and Solar Infrared-Station (SIRS) method, respectively, was developed and is currently being applied on a near-real-time basis. Because the nighttime algorithms are still being improved, only the daytime data are considered fully operational. The VISST cloud mask has been improved to discriminate between clouds and snow, and utilizes an improved parameterization of visible (0.65 μm) reflectance. This paper describes the results from the analysis of data taken since January 2000 on a half-hourly basis.

Methodology and Data

The Geostationary Operational Environmental Satellite (GOES)-8 1- and 4-km imager data (0.65 μm, visible [VIS]; 3.9 μm, SIR; 10.8 μm, infrared [IR]; and 12.0 μm, SWC) taken every 15 to 60 min are ingested as they become available using the Man-computer Interactive Data Analysis System (McIDAS). Minnis et al. (2002) discuss the calibration of the VIS radiances. Determination of the cloud properties requires an array of various input data. Clear-sky VIS reflectance at a given time and location are computed by applying solar-zenith-angle (SZA) dependent albedo models and bidirectional reflectance models to a database of clear-sky zenith-sun albedos resolved at 10' of latitude and longitude. A similar database for the surface emissivity ε_i at wavelengths i = 3.9, 10.8, and 12.0 μm is also maintained to predict the clear-sky temperatures for these channels at any given time and location (e.g., Smith et al. 1999). Water-land percentage and elevation maps are also used to determine the surface type and atmospheric thickness, respectively, for each grid location. Temperature and humidity profiles are interpolated from the gridded Rapid Update Cycle (RUC; Benjamin et al. 1994) forecast analyses to match the analysis grid and image times. Surface skin temperature T_s is estimated from the RUC surface air temperature following an update version of the technique used by Minnis et al. (1995a).

Each GOES-8 pixel is classified as clear or cloudy using a modified version of the cloud identification algorithm (e.g., Trepte et al. 1999) developed for the Clouds and Earth's Radiant Energy System (CERES). For each pixel, this method compares the observed VIS reflectance, IR temperature, and SIR-IR brightness temperature difference to several basic thresholds based on the predicted clear-sky values and their uncertainties for the grid box containing the pixel. In a simplified form, the clear-sky temperature for channel i is

$$B_i(T_i) = \varepsilon_{ai}B_i(T_{ai}) + (1-\varepsilon_{\square i})B_i(T_{si}),$$ (1)

where B is the Planck function, ε and T_a are the atmospheric effective emissivity and effective temperature, respectively. The radiance for the apparent surface radiating temperature, T_{si}, is

$$B_i(T_{si}) = \varepsilon_i\mu B_i(T_s) + (1-\varepsilon_i)[L_{ai} + \chi_k S_i],$$ (2)

where μ is the cosine of the viewing zenith angle (VZA), L_a is the downwelling atmospheric radiance at the surface, χ_k is the bidirectional reflectance factor for surface type k, and S is the downwelling solar radiance at the surface. The atmospheric absorption and emission are computed with a simple radiative transfer model using the correlated k-distribution coefficients from Minnis et al. (2002) and the temperature and humidity in each RUC layer.

Cloud properties are computed for each pixel identified as cloudy using the VISST, which is an upgrade of the VIS-SIR-IR method described by Minnis et al. (1995b). VISST computes an array of VIS reflectances and SIR, IR, and SWC temperatures at the top of atmosphere for the specified VZA, SZA, and relative azimuth angle using model lookup tables (Minnis et al. 1998) in parameterizations that account for the contributions of the surface and atmosphere to the radiance in each channel. Solutions are computed iteratively for liquid and ice clouds yielding effective droplet size effective radius (r_e) or effective ice crystal diameter D_e, optical depth τ, and cloud temperature T_c. Phase is determined using several criteria including the value of T_c, available solutions, and consistency with the observed SWC temperature. Ice water path (IWP) or liquid water path (LWP) is computed from the particle size and optical depth. Broadband shortwave albedo and outgoing longwave radiation are computed for each pixel from narrowband-to-broadband relationships derived from CERES data matched with GOES-8 imager data over the same region. Skin temperature is derived from the observed IR temperature for each clear pixel using Eqs. (1) and (2).

At night, the SIR-IR-SWC (SIRS) method is used to solve for the same parameters except no optical depths can be retrieved for clouds with $\tau > 10$. The IR temperatures change insignificantly for larger optical depths. Thus, for SZA > 78°, the information concerning the cloud microphysics is limited and default values are used for any optically thick cloud. The GOES data are analyzed with these techniques and later reprocessed using RUC reanalyses instead of the forecast data to provide improved accuracy in all the products.

Results

The results presented here are average values for a 4° box centered on the ARM SGP site near Lamont, Oklahoma. The mean daytime values of r_e and D_e are shown in Figure 1 for 0.5° regions within the 4° domain for all scenes containing clouds entirely liquid water or ice, respectively. Droplet radius varies from 9.4 to 12.0 μm with the larger droplets occurring in the southeastern portion of the grid. The effective ice diameters are more variable ranging 37 to 68 μm. The mean values of r_e and D_e for all liquid and ice clouds in all conditions are approximately 0.5 to 1.0 μm larger and 5 to 20 μm smaller, respectively, because of the effects of overlapping ice and water clouds (Kawamoto et al. 2001). The variability in D_e is large because, during July, ice clouds rarely occurred without water clouds in a given region. If all conditions are included, the range in mean values of D_e is between 35 and 55 μm.

The monthly mean daytime liquid and ice cloud optical depths in Figure 2 track each other fairly closely except during January 2000 when τ_{ice} is less than half the value of τ_{liq}. Maximum mean optical depth occurred during March, while the minimum was observed during August. The optical depths are
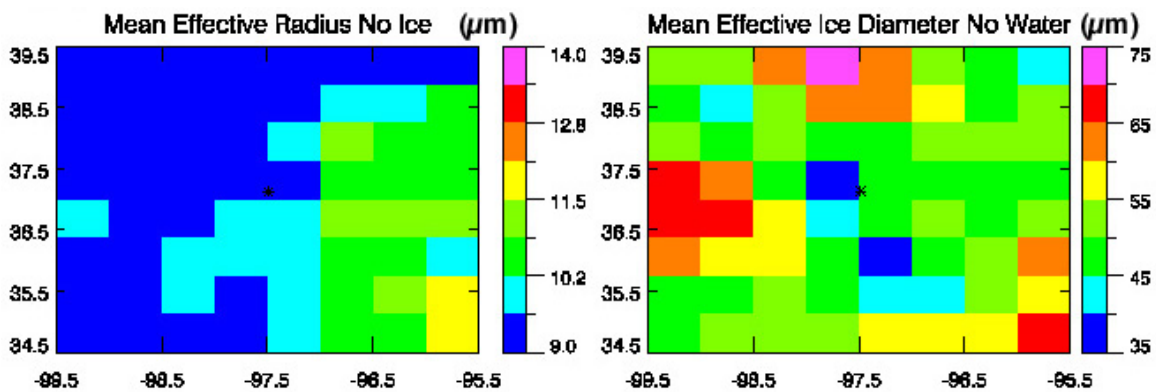

Figure 1. Mean daytime cloud effective particle sizes for July 2000 from GOES-8 data.
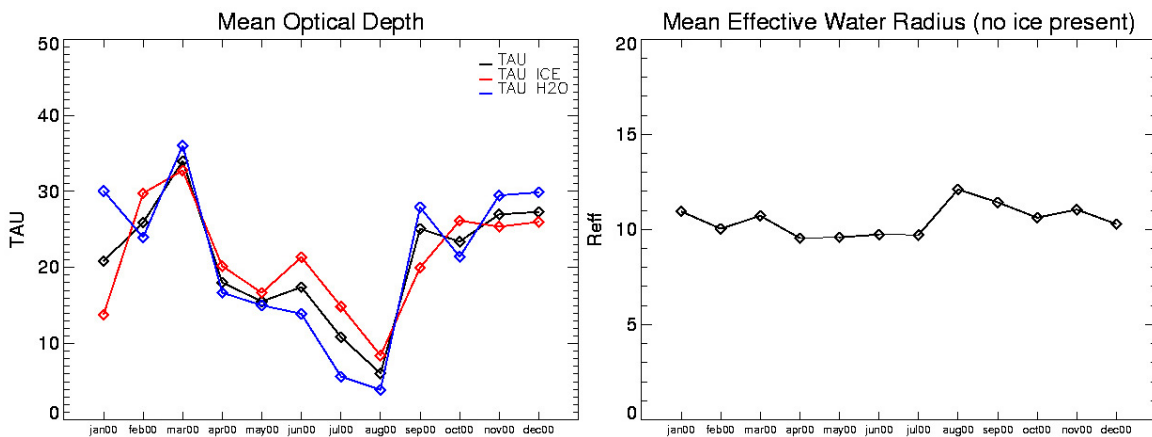

Figure 2. Monthly mean daytime cloud properties for 4° domain during 2000. Reff is r_e in μm.

computed for the phase determined for each pixel. The ice clouds may often occur over liquid water clouds. The ice cloud optical depth may be an overestimate and the liquid water optical depth may be underestimated on average. Nevertheless, the mean optical depth shown in Figure 2 should provide a good representation of the monthly variation during daylight hours. The monthly mean daytime effective droplet radius for ice-free conditions, also shown in Figure 2, varies by ~3 μm over the year. The minimum occurs during late spring while the maximum is observed during August when the optical depth is at a minimum. The droplet sizes in Figure 2 are about 2 μm larger than those derived from surface radar data for stratus clouds over the SGP Central Facility (Dong et al. 2000), a result consistent with the comparisons of Dong et al. (2002). Differences between the two estimates of r_e are due to several factors. Thin cirrus clouds not detected over the low clouds cause an increase in r_e. Pixels containing broken cloud scenes interpreted as overcast clouds cause an increase in r_e. Also, the signal from the 3.7-μm channel used for deriving r_e generally comes from the top layers of the cloud where the droplets are often largest. A direct comparison of the radar values using only satellite data with no ice and 100% cloud cover would eliminate the first two factors. The effect of the vertical structure of r_e can then be isolated. The larger values of r_e during August 2000 are most likely due to the broken cloud effect as the mean cloud optical depth is relatively small, a condition associated with pixels having broken clouds (Nguyen et al. 2002). The seasonal variation in D_e (not shown) is more erratic, especially when all liquid contaminated data are removed.

The results are also useful for studying the diurnal variation in cloud properties over the domain. For example, Figure 3 indicates that the mean LWP and IWP over the 4° domain peak in the early morning during winter and summer with a secondary maximum during the afternoon. The nearly constant values during the night in Figure 3 result from using default values of particle size and optical depth for clouds with $\tau > 6$. The diurnal variations in Figure 3 are consistent with nocturnal maxima in the development of precipitating systems, which would dominate the monthly values of IWP or LWP.

Discussion and Future Research

The results presented here are a brief summary of the data products available. Pixel-level data are available within the 4° box in Figure 1, while 0.5° grid box averages of each property and radiance are available every half hour for the large SGP domain covering the area bounded by 32°N, 42°N, 91°W, and 105°W. The pixel-level data from this large domain are converted to image files available in near-real time at http://www-angler.larc.nasa.gov/armsgp/ or through http://www-pm.larc.nasa.gov/. Also available at the latter site, is near-real-time GOES-8 spectral and multi-spectral imagery for the SGP domain and other parts of the United States.

These products represent the first attempt at providing a wide range of useful cloud properties in a timely fashion. Initial validation studies using ARM surface datasets have revealed areas where improvement is warranted and possible. Nguyen et al. (2002) are exploring a multi-resolution method to account for sub-pixel fractional cloud cover and reduce the bias in some of the parameters for broken cloud fields. Kawamoto et al. (2001) and Arduini et al. (2002) are developing techniques to identify and analyze pixels with overlapped, multi-layered clouds. Heck et al. (2002) are examining new approaches to improving the detection and analysis of clouds observed at low sun elevation angles and during the night. Khaiyer et al. (2002) have been improving the conversion of narrowband radiances to broadband
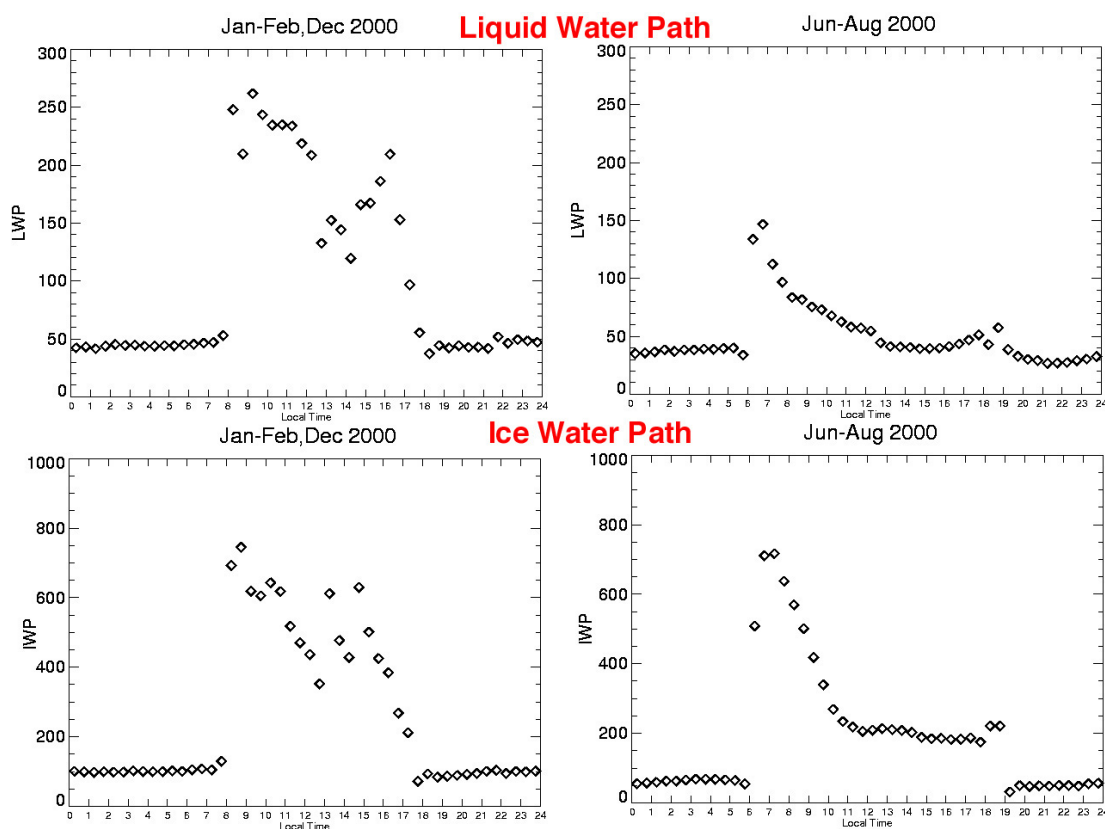
Figure 3. Seasonal mean hourly LWP and IWP over the 4° SGP domain during 2000.

fluxes and constructing new algorithms to compute skin temperature at night and in cloudy conditions. Chakrapani et al. (2002) are using ARM surface data to help develop new methods for estimating cloud thickness from the VISST retrievals. Validation efforts are continuing. As new or updated algorithms become available, they will be incorporated into the near-real time and archival product processing.

In addition to the climatological importance of the long-term products for large-scale model validation, the near-real time results should be valuable for planning and executing flight missions over the SGP and for validating forecasts from cloud-resolving models. These products should also be useful for incorporation into model assimilations for forecast initialization and for constructing accurate three-dimensional characterizations of clouds over the SGP domain.

Corresponding Author

P. Minnis, p.minis@larc.nasa.gov, (757) 864-5671

References

Arduini, R. F., P. Minnis, and D. F. Young, 2002: Investigation of a visible reflectance parameterization for determining cloud properties in multi-layered clouds. *Proc. AMS 11ᵗʰ Conf. Cloud Physics*, June 3-7, Ogden, Utah.

Benjamin, S. G., K. J. Brundage, and L. L. Morone, 1994: *The Rapid Update Cycle. Part I: Analysis/model description*. Technical Procedures Bulletin No. 416, NOAA/NWS, p. 16.

Chakrapani, V., D. R. Doelling, A. D. Rapp, and P. Minnis, 2002: Cloud thickness estimation from GOES-8 satellite data over the ARM SGP site. This proceedings.

Dong, X., P. Minnis, T. P. Ackerman, E. E. Clothiaux, G. G. Mace, R. N. Long, and J. C. Liljegren, 2000: A 25-month database of stratus cloud properties generated from ground-based measurements at the ARM SGP site. *J. Geophys. Res.*, **105**, 4529-4537.

Dong, X., P. Minnis, G. G. Mace, W. L. Smith Jr., M. Poellot, and R. Marchand, 2002: Comparison of stratus cloud properties deduced from surface, GOES, and aircraft data during the March 2000 ARM Cloud IOP. *J. Atmos. Sci.*, accepted.

Heck, P. W., A. D. Rapp, P. Minnis, W. L. Smith, Jr., and L. Nguyen, 2002: An improved technique for retrieval of cloud properties at night and in low sun conditions. This proceedings.

Kawamoto, K., P. Minnis, and W. L. Smith, Jr., 2001: Cloud overlapping detection algorithm using solar and ir wavelengths with GOES data over ARM/SGP site. In *Proceedings of the Eleventh Atmospheric Radiation Measurement (ARM) Science Team Meeting*.

Khaiyer, M. M., P. Minnis, W. L. Smith, Jr., A. D. Rapp, D. R. Doelling, and L. Nguyen, 2002: Evaluation of a 5-year cloud and radiative property dataset derived from GOES-8 data over the Southern Great Plains. This proceedings.

Minnis, P., D. P. Garber, D. F. Young, R. F. Arduini, and Y. Takano, 1998: Parameterization of reflectance and effective emittance for satellite remote sensing of cloud properties. *J. Atmos. Sci.*, **55**, 3313-3339.

Minnis, P., D. P. Kratz, J. A. Coakley, Jr., M. D. King, D. Garber, P. Heck, S. Mayor, D. F. Young, and R. Arduini, 1995b: Cloud Optical Property Retrieval (Subsystem 4.3). "Clouds and the Earth's Radiant Energy System (CERES) Algorithm Theoretical Basis Document, Volume III: Cloud Analyses and Radiance Inversions (Subsystem 4)," *NASA RP 1376 Vol. 3*, edited by CERES Science Team, pp. 135-176.

Minnis, P., L. Nguyen, D. F. Young, D. R. Doelling, D. P. Kratz, and W. F. Miller, 2002: Rapid calibration of operational and research meteorological satellite imagers, Part I: Use of research satellite visible channels as references. *J. Atmos. Oceanic Technol.,* in press.

Minnis P., W. L. Smith, Jr., D. P. Garber, J. K. Ayers, and D. R. Doelling, 1995a: "Cloud properties derived from GOES-7 for Spring 1984 ARM Intensive Observing Period using Version 1.0.0 of ARM satellite data analysis program." *NASA RP 1366*, p. 58.

Nguyen, L., P. Minnis, D. F. Young, W. L. Smith, Jr., A. D. Rapp, P. W. Heck, and M. M. Khaiyer, 2002: Use of multi-resolution imager data to account for partially cloud-filled pixels. This proceedings.

Smith, W. L., Jr., P. Minnis, D. F. Young, and Y. Chen, 1999: Satellite-derived surface emissivity for ARM and CERES. *Proc. AMS 10th Conf. Atmos. Rad.*, June 28–July 2, 410-413, Madison, Wisconsin.

Trepte, Q., Y. Chen, S. Sun-Mack, P. Minnis, D. F. Young, B. A. Baum, and P. W. Heck, 1999: Scene identification for the CERES cloud analysis subsystem. *Proc. AMS 10th Conf. Atmos. Rad.*, June 28-July 2, 1999, 169-172, Madison, Wisconsin.